Article

Geminal *J* Spin–Spin Coupling Constants as Probes of the Glycosidic Torsion Angle in Oligosaccharides

Thomas E. Klepach, Ian Carmichael, and Anthony S. Serianni

J. Am. Chem. Soc., **2005**, 127 (27), 9781-9793• DOI: 10.1021/ja040251y • Publication Date (Web): 16 June 2005

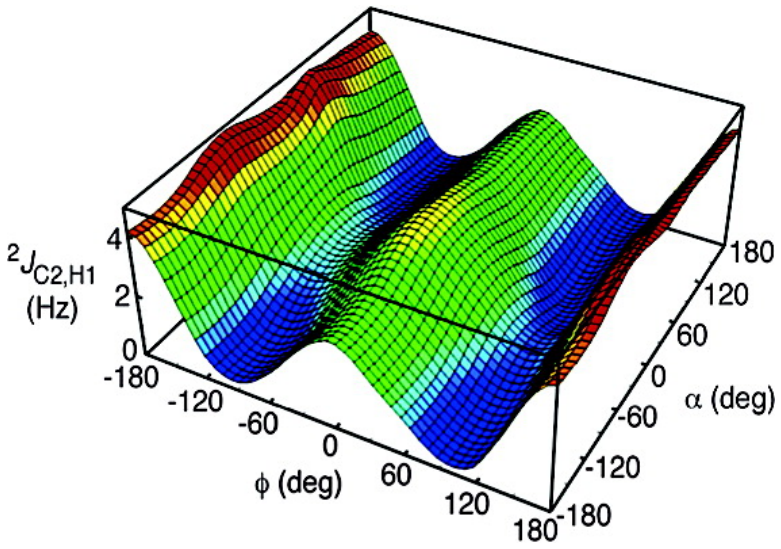

More About This Article

Additional resources and features associated with this article are available within the HTML version:

- Supporting Information
- Links to the 4 articles that cite this article, as of the time of this article download
- Access to high resolution figures
- Links to articles and content related to this article
- Copyright permission to reproduce figures and/or text from this article

View the Full Text HTML

Journal of the American Chemical Society is published by the American Chemical Society. 1155 Sixteenth Street N.W., Washington, DC 20036

J|A|C|S
ARTICLES
Published on Web 06/16/2005

Geminal $^2J_{CCH}$ Spin−Spin Coupling Constants as Probes of the ϕ Glycosidic Torsion Angle in Oligosaccharides

Thomas E. Klepach,[†] Ian Carmichael,[‡] and Anthony S. Serianni*,[†]

Contribution from the Department of Chemistry and Biochemistry and Radiation Laboratory, University of Notre Dame, Notre Dame, Indiana 46556-5670

Received November 8, 2004; E-mail: serianni.1@nd.edu

Abstract: Two-bond $^{13}C-^1H$ NMR spin−spin coupling constants ($^2J_{CCH}$) between C2 and H1 of aldopyranosyl rings depend not only on the relative orientation of electronegative substituents on the C1−C2 fragment but also on the C−O torsions involving the same carbons. The latter dependencies were elucidated theoretically using density functional theory and appropriate model pyranosyl rings representing the four relative configurations at C1 and C2, and a 2-deoxy derivative, to probe the relationship between $^2J_{C2,H1}$ magnitude and sign and the C1−O1 (phi, ϕ) and C2−O2 (α) torsion angles. Related calculations were also conducted for the reverse coupling pathway, $^2J_{C1,H2}$. Computed *J*-couplings were validated by comparison to experimentally measured couplings. $^2J_{CCH}$ displays a primary dependence on the C−O torsion involving the carbon bearing the coupled proton and a secondary dependence on the C−O torsion involving the coupled carbon. These dependencies appear to be caused mainly by the effects of oxygen lone pairs on the C−H and C−C bond lengths along the C−C−H coupling pathway. New parameterized equations are proposed to interpret $^2J_{C1,H2}$ and $^2J_{C2,H1}$ in aldopyranosyl rings. The equation for $^2J_{C2,H1}$ has particular value as a potential NMR structure constraint for the C1−O1 torsion angle (ϕ) comprising the glycosidic linkages of oligosaccharides.

Introduction

Heteronuclear vicinal (three-bond) $^{13}C-^1H$ spin−spin coupling constants ($^3J_{CCCH}$ and $^3J_{COCH}$) are finding increased use as structure constraints in the conformational analysis of saccharides in solution due to their expected Karplus-like dependencies.[1−5] In contrast, geminal (two-bond) $^{13}C-^1H$ *J*-couplings ($^2J_{CCH}$) are less appreciated, although qualitative rules governing their dependencies on saccharide structure have been reported based on patterns of electronegative atom substitution in the C−C−H fragment.[6−8] Two key differences distinguish the C−C torsional dependencies of $^2J_{CCH}$ and $^3J_{CCCH}$. The ^2J dependencies are unimodal, whereas the ^3J dependencies are bimodal; one minimum and one maximum are observed in plots of $^2J_{CCH}$ versus C−C torsion compared to two minima and two maxima in plots of $^3J_{CCCH}$ versus C−C torsion. This difference confers advantages to $^2J_{CCH}$ since a reduced number of potential conformers exist that correspond to a particular coupling, thus potentially improving conformational analyses, especially in flexible systems. In saccharides, $^2J_{CCH}$ can be positive or negative in sign, often changing sign within a given torsional regime, whereas the signs of $^3J_{CCCH}/^3J_{COCH}$ are positive. Thus, if signs are taken into account, comparable dynamic ranges (~8 Hz) are observed for both types of coupling.

Recent studies of exocyclic hydroxymethyl group (CH_2OH) conformation in this laboratory have described the effect of C−C and C−O bond rotation on $^2J_{CCH}$ in saccharides.[9] In addition to their expected unimodal dependence on ω (O5−C5−C6−O6 torsion), $^2J_{C5,H6R}$ and $^2J_{C5,H6S}$ were found to exhibit significant secondary dependencies on θ (C5−C6−O6−OH6 torsion) (Figure 1 and Chart 1, structure **I**) (i.e., rotation of the C−O bond on the carbon bearing the coupled proton influenced $^2J_{CCH}$ significantly). The latter dependence is probably caused in part by changes in C6−H6*R*/*S* bond lengths induced by specific dispositions of the O6 lone pairs (i.e., rotation of the C6−O6 bond modulates the syn/anti orientation of lone pairs with respect to these C−H bonds, with anti orientations elongating the bonds).[10] Other studies have shown[9] that rotation of the C−O bond on the *coupled carbon* exerts a smaller effect on $^2J_{CCH}$. These C−O torsional effects are generalized in Chart 1 (structure **II**; C−C−H coupling pathway shown in blue); $^2J_{CCH}$ displays a primary dependence on a C−O rotamer if the oxygen of that rotamer is geminal to the coupled proton (β rotation) and a secondary dependence on a C−O rotamer if the carbon of that rotamer is the coupled carbon (α rotation).

[†] Department of Chemistry and Biochemistry.
[‡] Radiation Laboratory.

(1) Tvaroska, I.; Hricovini, H.; Petrakova, E. *Carbohydr. Res.* **1989**, *189*, 359−362.
(2) Mulloy, B.; Frenkiel, T. A.; Davies, D. B. *Carbohydr. Res.* **1988**, *184*, 39−46.
(3) Tvaroska, I.; Gadjos, J. *Carbohydr. Res.* **1995**, *271*, 151−162.
(4) Tvaroska, I.; Taravel, F. R.; Utille, J. P.; Carver, J. P. *Carbohydr. Res.* **2002**, *337*, 353−367.
(5) Cloran, F.; Carmichael, I.; Serianni, A. S. *J. Am. Chem. Soc.* **1999**, *121*, 9843−9851.
(6) Bock, K.; Pedersen, C. *Acta Chem. Scand.* **1977**, *B31*, 354−358.
(7) Schwarcz, J. A.; Perlin, A. S. *Can. J. Chem.* **1972**, *50*, 3667−3676.
(8) Schwarcz, J. A.; Cyr, N.; Perlin, A. S. *Can. J. Chem.* **1975**, *53*, 1872−1875.
(9) Thibaudeau, C.; Stenutz, R.; Hertz, B.; Klepach, T.; Zhao, S.; Wu, Q.; Carmichael, I.; Serianni, A. S. *J. Am. Chem. Soc.* **2004**, *126*, 15668−15685.
(10) (a) Stenutz, R.; Carmichael, I.; Widmalm, G.; Serianni, A. S. *J. Org. Chem.* **2002**, *67*, 949−958. (b) Serianni, A. S.; Wu, J.; Carmichael, I. *J. Am. Chem. Soc.* **1995**, *117*, 8645−8650.

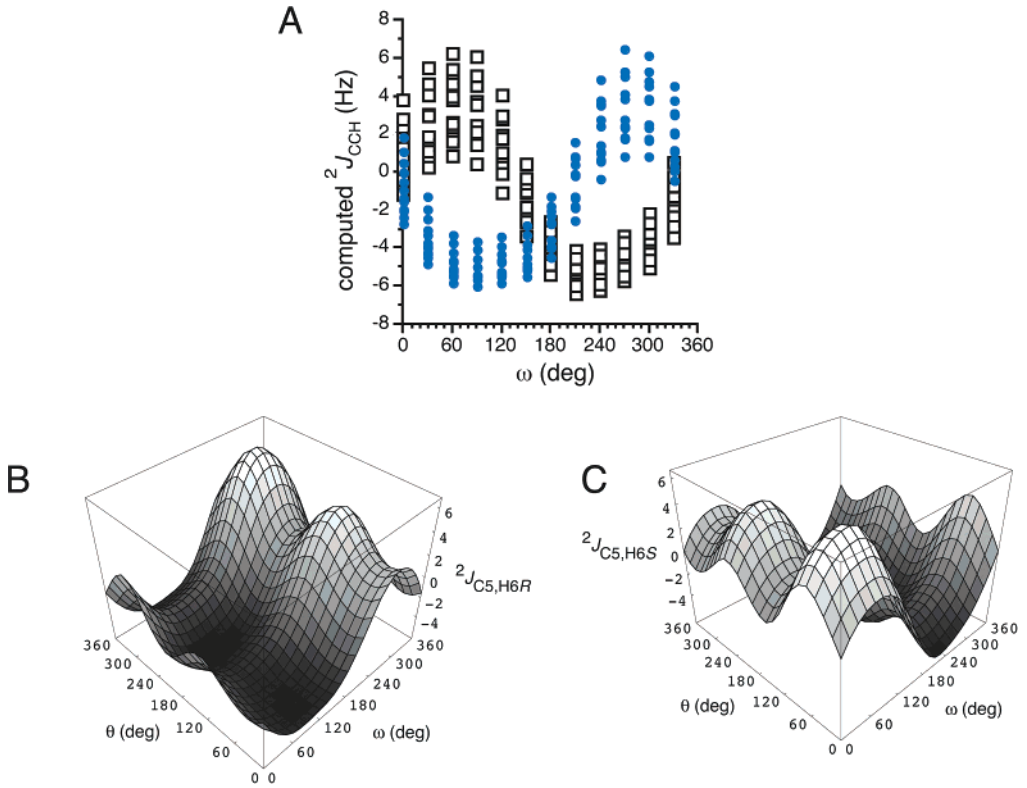

Figure 1. (A) Plot of computed $^2J_{C5,H6R}$ and $^2J_{C5,H6S}$ in **I** (Chart 1) as a function of ω (defined as the O5−C5−C6−O6 torsion angle). The scatter of points at discrete values of ω is caused by the effect of θ (defined as the C5−C6−O6−H torsion angle). Note the unimodal behavior with respect to ω. Closed blue circles, $^2J_{C5,H6R}$; open black squares, $^2J_{C5,H6S}$. (B) Hypersurface showing the effect of ω and θ on $^2J_{C5,H6R}$ in **I**. (C) Hypersurface showing the effect of ω and θ on $^2J_{C5,H6S}$ in **I**. Data taken from ref 9.

Chart 1

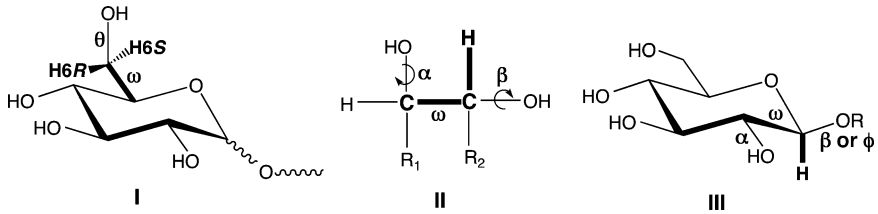

Armed with these results and arguing by analogy, we posed the question addressed in this report, namely, might $^2J_{CCH}$ serve as a probe of the phi (ϕ) glycosidic torsion angle in oligosaccharides (Chart 1, structure **III**; C−C−H coupling pathway indicated in blue)? In this case, contributions from ω can be ignored because the C1−C2 bond torsion is constrained by the ring, leaving $^2J_{C2,H1}$ affected by α (C2−O2 bond torsion) and β/ϕ rotations (C1−O1 bond torsion). Note that ϕ and β are redundant. We investigated this possibility by conducting density functional theory (DFT) calculations on model structures **1**−**8** (Chart 2) designed to capture the effect of C1 and C2 structure and configuration on $^2J_{C2,H1}$ magnitude and sign. As a control, we also studied the reverse coupling pathway, $^2J_{C1,H2}$, in the same structures. Computed couplings were validated by comparison to experimental $^2J_{C1,H2}$ and $^2J_{C2,H1}$ in aldopyranosyl rings having different structures and configurations. We show herein that $^2J_{C2,H1}$ values display a significant and systematic dependence on ϕ in glycosides regardless of the relative configuration at C1 and C2 of the aldopyranosyl ring. These findings have important implications for conformational studies of the glycosidic and nonglycosidic C−O torsion angles of saccharides in solution.

Computations

Geometry optimizations were conducted as a function of varying only ϕ (defined as the O5−C1−O1−CH_3 torsion angle) in **1**−**4**, or both ϕ and α (defined as the C1−C2−O2−H torsion angle) in **5**−**8**, in 30° increments over the range 0−360°, yielding 12 structures for **1**−**4** and 144 structures for **5**−**8**. Geometry optimizations using DFT were performed using the B3LYP hybrid functional[11] and the 6-31G* basis set[12] within *Gaussian*98.[13a] Coupling constants $^2J_{C1,H2}$ and $^2J_{C2,H1}$ were computed as described previously[5] using the standard B3LYP functional, finite-field perturbation theory implemented within *Gaussian*94,[13b] and an extended basis set ([5s2p1d|3s1p])[10a] designed to reliably recover the Fermi contact contribution to the coupling. Equations describing the dependencies of both *J*-couplings on ϕ and/or α were parameterized using the least-squares Monte Carlo fitting module within *ProFit 5.6.2* (Quantum Soft, Zürich, Switzerland).

A series of geometry optimizations and *J*-coupling calculations was also conducted on **5**−**8** in which $r_{C1,H1}$, $r_{C2,H2}$, or $r_{C1,C2}$ were varied in 0.001 Å increments about the respective average optimized bond length observed in the above ϕ/α hypersurfaces, covering an overall range of ∼0.02 Å. In these calculations, ϕ and α were held constant at values

(11) Becke, A. D. *J. Chem. Phys.* **1993**, *98*, 5648−5652.
(12) Hehre, W. J.; Ditchfield, R.; Pople, J. A. *J. Chem. Phys.* **1972**, *56*, 2257−2261.

Chart 2

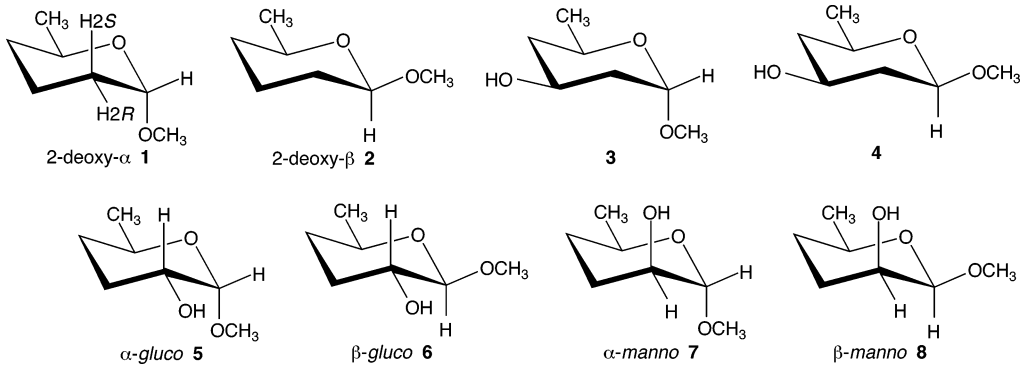

observed in the lowest energy structures of the total energy hypersurface (ϕ/α for **5**, 60°/−60°; for **6**, −60°/60°; for **7**, 60°/60°; for **8**, −60°/−60°; see below). These calculations were performed to evaluate the effect of these bond lengths on $^1J_{CH}$ and $^2J_{CCH}$ values; all other molecular parameters in the structures were geometrically optimized, although the induced changes in a given bond length affected these optimized parameters minimally (e.g., changing $r_{C1,H1}$ exerted little effect on other nearby or remote bond lengths or angles).

Results and Discussion

A. Energetics. The effect of C1−O1 bond rotation (ϕ) on the total energies E of **1** and **2** is shown in Figure 2. For **1**, $E_{\phi\ 60°} < E_{\phi\ 180°} < E_{\phi\ -60°}$, whereas for **2**, $E_{\phi\ -60°} < E_{\phi\ 60°} < E_{\phi\ 180°}$. In both cases, the most stable ϕ rotamer orients the aglycone methyl carbon anti to C2, as predicted by the exoanomeric effect.[14] The relative stabilities of the remaining two ϕ rotamers are reversed in **1** and **2**, behavior presumably caused by a combination of stereoelectronic and steric effects. In **1**, $\phi = -60°$ is destabilized for steric reasons (the aglycone is oriented below the ring), while in **2**, $\phi = 180°$ is destabilized by eclipsed lone-pair interactions between O1 and O5. Curve amplitude for **1** appears slightly greater than that for **2**, suggesting greater ϕ flexibility in **2**. Since **1** and **2** lack a C2 hydroxyl group, potential effects caused by C2 substitution are absent.

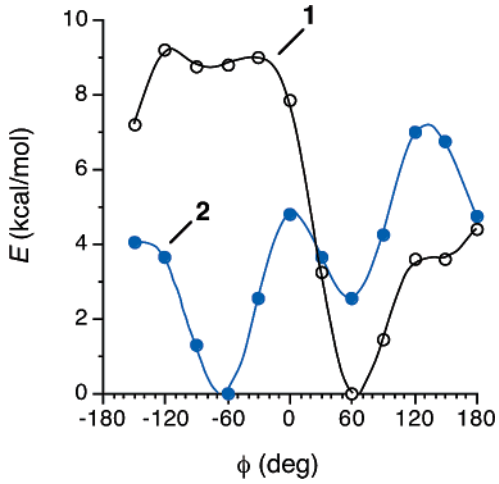

Figure 2. Plot showing the effect of ϕ on the calculated total energy E of **1** and **2** determined by DFT (B3LPY/6-31G*, in vacuo).

The effect of C2−O2 bond rotation (α) on the relative energies of ϕ rotamers in **5**−**8** is shown in Figure 3. For a specific ϕ torsion, variations in E caused by 360° α rotations vary from 3 to 6 kcal/mol, and the magnitude of variation depends somewhat on ϕ. Consideration of only perfectly staggered α rotamers yields a more limited variation and the emergence of a lowest energy pathway for ϕ rotation in **5**−**8**. In **5**, $E_{\phi\ 60°} < E_{\phi\ 180°} < E_{\phi\ -60°}$, whereas in **6**, $E_{\phi\ -60°} < E_{\phi\ 60°} < E_{\phi\ 180°}$. These trends mimic those observed in **1** and **2**, respectively, although curve amplitude is slightly greater in **5** and **6**.

Data for **7** and **8** are similar to those for **5** and **6** (Figure 3C,D). Interestingly, α rotation (staggered rotamers only) in **8** appears to affect E more significantly than observed for **5**−**7**. As observed in **5** and **6**, the relative energies of the lowest energy pathways for **7** and **8** are similar to those observed in **1** and **2**, respectively; curve amplitudes for **2** and **8** are virtually identical. Importantly, correlations between ϕ and E in **5**−**8** appear similar for each of the three staggered α rotamers (the curves are *y*-shifted but otherwise similar in shape).

Correlations between ϕ, α, and E in **5**−**8** were also inspected in plots of E versus α (Figure 4). Scatter is greater than observed in Figure 3 since ϕ rotation causes a greater change in E than does α rotation. If only staggered ϕ rotamers are considered, minimal energy pathways emerge. Interestingly, the three curves for each structure are not only *y*-shifted, but also change in shape in some cases (i.e., the influence of α on E depends on the

(13) (a) Frisch, M. J.; Trucks, G. W.; Schlegel, H. B.; Scuseria, G. E.; Robb, M. A.; Cheeseman, J. R.; Zakrzewski, V. G.; Montgomery, J. A., Jr.; Stratmann, R. E.; Burant, J. C.; Dapprich, S.; Millam, J. M.; Daniels, A. D.; Kudin, K. N.; Strain, M. C.; Farkas, O.; Tomasi, J.; Barone, V.; Cossi, M.; Cammi, R.; Mennucci, B.; Pomelli, C.; Adamo, C.; Clifford, S.; Ochterski, J.; Petersson, G. A.; Ayala, P. Y.; Cui, Q.; Morokuma, K.; Malick, D. K.; Rabuck, A. D.; Raghavachari, K.; Foresman, J. B.; Cioslowski, J.; Ortiz, J. V.; Baboul, A. G.; Stefanov, B. B.; Liu, G.; Liashenko, A.; Piskorz, P.; Komaromi, I.; Gomperts, R.; Martin, R. L.; Fox, D. J.; Keith, T.; Al-Laham, M. A.; Peng, C. Y.; Nanayakkara, A.; Challacombe, M.; Gill, P. M. W.; Johnson, B.; Chen, W.; Wong, M. W.; Andres, J. L.; Gonzalez, C.; Head-Gordon, M.; Replogle, E. S.; Pople, J. A. *Gaussian98*; revision A.9, Gaussian, Inc.: Pittsburgh, PA, 1998. (b) Frisch, M. J.; Trucks, G. W.; Schlegel, H. B.; Gill, P. M. W.; Johnson, B. G.; Robb, M. A.; Cheeseman, J. R.; Keith, T.; Petersson, G. A.; Montgomery, J. A.; Raghavachari, K.; Al-Laham, M. A.; Zakrzewski, V. G.; Ortiz, J. V.; Foresman, J. B.; Peng, C. Y.; Ayala, P. Y.; Chen, W.; Wong, M. W.; Andres, J. L.; Replogle, E. S.; Gomperts, R.; Martin, R. L.; Fox, D. J.; Binkley, J. S.; Defrees, D. J.; Baker, J.; Stewart, J. P.; Head Gordon, M.; Gonzalez, C.; Pople, J. A. *Gaussian94*; Gaussian, Inc.: Pittsburgh, PA, 1995.

(14) (a) Thøgersen, H.; Lemieux, R. U.; Bock, K.; Meyer, B. *Can. J. Chem.* **1982**, *60*, 44−57. (b) Tvaroska, I.; Bleha, T. *Adv. Carbohydr. Chem. Biochem.* **1989**, *47*, 45−123. (c) Meyer, B. Conformational Aspects of Oligosaccharides. In *Carbohydrate Chemistry*; Thiem, J., Ed.; Topics in Current Chemistry 154; Springer-Verlag: Berlin, Heidelberg, 1990; pp 141−208. (d) Juaristi, E.; Cuevas, G. *The Anomeric Effect*; CRC Press: Boca Raton, FL, 1995. (e) Kirby, A. J. *The Anomeric Effect and Related Stereoelectronic Effects at Oxygen*; Springer: New York, 1983. (f) Lemieux, R. U.; Koto, S. *Tetrahedron* **1974**, *30*, 1933−1944. (g) Praly, J.-P.; Lemieux, R. U. *Can. J. Chem.* **1987**, *65*, 213−223. (h) Lemieux, R. U. *Pure Appl. Chem.* **1971**, *25*, 527−548.

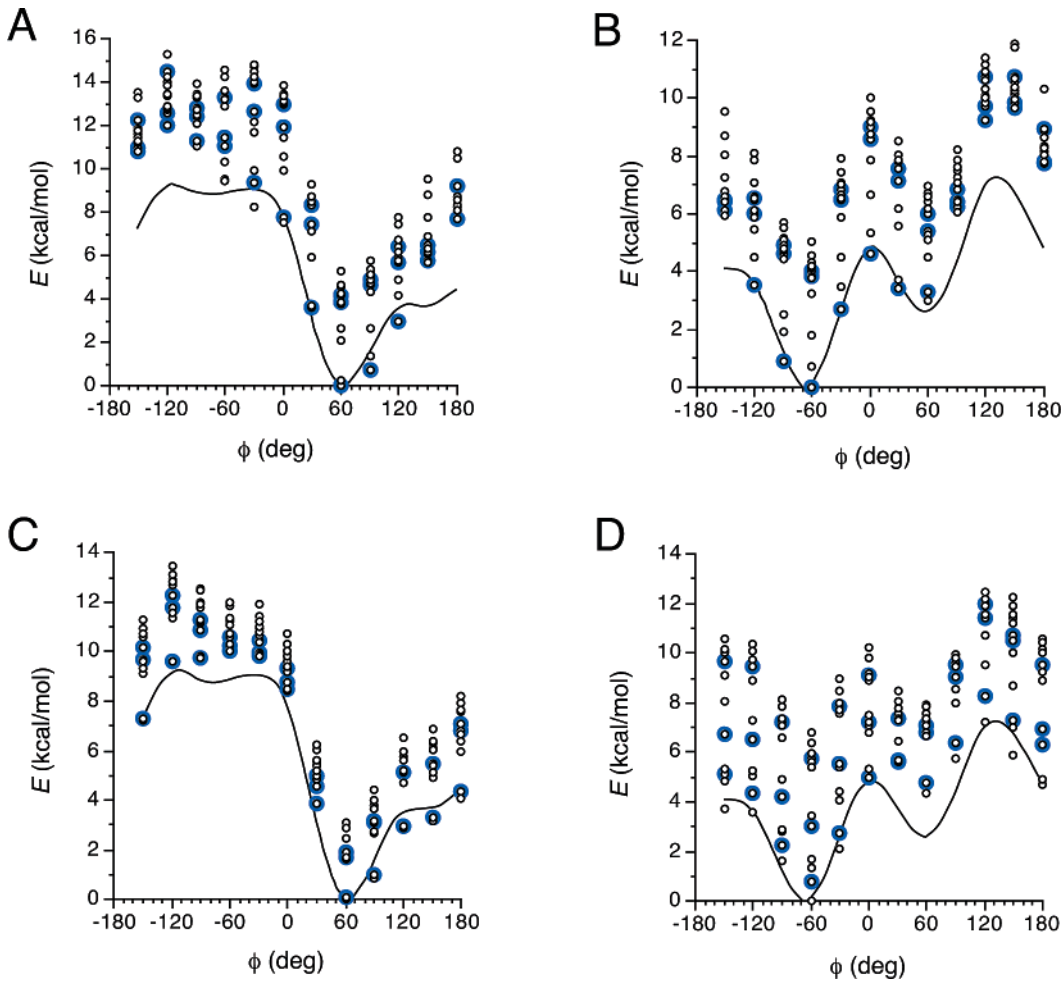

Figure 3. Plots showing the effect of ϕ on the calculated total energy E of **5** (A), **6** (B), **7** (C), and **8** (D) determined by DFT (B3LYP/6-31G*, in vacuo). The scatter of points at discrete values of ϕ is caused by the effect of α; data points in blue are for perfectly staggered values of α. Superimposed on each plot is the corresponding curve derived from either **1** (A and C) or **2** (B and D).

value of ϕ due to H-bonding between O1H and O2H). From these data, the most stable ϕ/α combinations in **5**−**8** were identified: **5**, 60°/−60°; **6**, −60°/60°; **7**, 60°/60°; **8**, −60°/−60°. Not unexpectedly, these conformers are characterized by the presence of intramolecular hydrogen bonding, which in gas-phase calculations confers differential stability to conformers that contain them. Whether these ϕ/α combinations are indeed the most populated states in aqueous solution is an interesting question but one of peripheral importance to the present work, provided that the presence of H-bonding in some structures does not adversely affect the parameterization of $^2J_{CCH}$ equations. The latter issue is discussed further below. Contour plots of populations computed from the data in Figures 3 and 4 are provided in Supporting Information (Figure S1). If an arbitrary 2 kcal/mol cutoff is applied, data in Figure 4 indicate that **7** experiences greater variability in the preferred C2−O2 torsion at the most stable C1−O1 torsion than **5**, **6**, and **8** (i.e., C2−O2 torsions of 60° and −60° are within 2 kcal/mol in this structure). The reduced interactions between O1 and O2 in **7** caused by their trans relationship apparently lead to this greater flexibility.

B. $^2J_{CCH}$ Spin-Couplings in 1−4. $^2J_{C1,H2R}$ and $^2J_{C1,H2S}$ in **1** and **2** were calculated as a function of ϕ, and potential effects of oxygen substitution at C3 were inspected from similar calculations conducted on **3** and **4** (Figure 5). Adding an equatorial oxygen at C3 causes only a minor change (<0.2 Hz) in $^2J_{C1,H2R/S}$[15] and $^2J_{C2,H1}$, and overall shape is conserved. Although not studied explicitly, similar results are expected for an axial O3.

Calculated $^2J_{C1,H2R}$ and $^2J_{C1,H2S}$ are similar in magnitude in **1**/**3** (0 to −3.5 Hz) (Figure 5A) and change by ∼2 Hz upon 360° rotation about ϕ. In contrast, $^2J_{C1,H2R}$ (−1.4 to −2.4 Hz) (Figure 5B) and $^2J_{C1,H2S}$ (−6.6 to −7.6 Hz) (Figure 5C) differ significantly in **2**/**4** and change by ∼1 Hz upon 360° rotation about ϕ. $^2J_{C1,H2R/S}/\phi$ curves for **1**/**3** and **2**/**4** appear approximately unimodal.

Calculated $^2J_{C2,H1}$ in **1**/**3** and **2**/**4** change significantly upon 360° rotation about ϕ (∼4 Hz) (Figure 5D,E). In both anomeric configurations, the calculated coupling is positive in sign, with the coupling being more positive (3−7 Hz) in **2**/**4** than that in **1**/**3** (0−4 Hz). In contrast to $^2J_{C1,H2R/S}$, $^2J_{C2,H1}/\phi$ curves are bimodal.

Calculated $^2J_{CCH}$ values were compared to experimental couplings measured in methyl 2-deoxy-α- (**9**) and 2-deoxy-β-D-*arabino*-hexopyranoses (**10**) (Chart 3).[16] Overall trends are maintained in the calculated and experimental couplings, but

(15) Note that the axial H2 (H2a) is H2*S*, and the equatorial H2 (H2e) is H2*R* in **1**−**4** (see Chart 2).
(16) Bandyopadhyay, T.; Wu, J.; Serianni, A. S. *J. Org. Chem.* **1993**, *58*, 5513−5517.

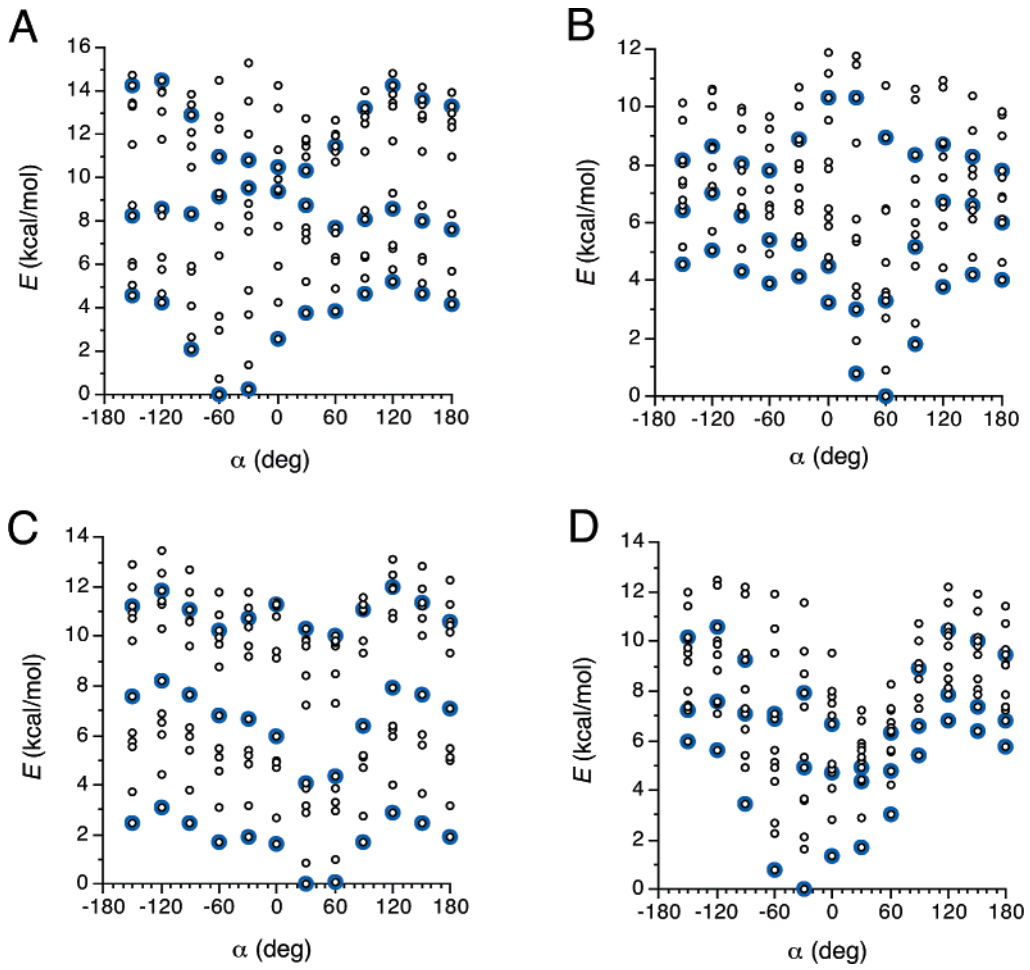

Figure 4. Plots showing the effect of α on the calculated total energy *E* of **5** (A), **6** (B), **7** (C), and **8** (D) determined by DFT (B3LYP/6-31G*, in vacuo). The scatter of points at discrete values of α is caused by the effect of ϕ; data points in blue are for perfectly staggered values of ϕ.

absolute magnitudes show some differences. The latter deviations are attributed to ring substitution effects, limitations in the methodology used to calculate the couplings, and/or effects of solution averaging and solvation on the experimental couplings.

Bond lengths in the vicinity of the anomeric carbons of **1** and **2** were examined as a function of ϕ. As expected from stereoelectronic considerations,[17] $r_{C1,O1}$ and $r_{C1,O5}$ exhibit complementary behavior, with the former and latter showing two minima and maxima, respectively, at $\phi = \sim 60°$ and $\sim -60°$ (Figure 6). The general behavior of $r_{C1,O5}$ is very similar in **1** and **2**, whereas the global minimum for $r_{C1,O1}$ shifts from $\phi = \sim 60°$ in **1** to $\phi = \sim -60°$ in **2**. This shift is coincident with the shift in the global energy minimum from **1** to **2** (Figure 2). The exocyclic C1−O1 bond length depends on bond orientation, with the equatorial orientation in **2** exhibiting substantially shorter bond lengths. In contrast, $r_{C1,O5}$ is slightly larger in **2** than in **1**.

Bond lengths $r_{C1,H1}$ and $r_{C1,C2}$ exhibit two minima upon rotation of ϕ through 360° (Figure 7), as observed for $r_{C1,O1}$ and $r_{C1,O5}$. In the most stable conformers of **1** and **2**, $r_{C1,O1}$ and $r_{C1,C2}$ are minimal (or near minimal), whereas $r_{C1,H1}$ and $r_{C1,O5}$ are maximal (or near maximal). The magnitude of $^2J_{C2,H1}$ in **1** and **2** approximately tracks r_{C1-H1}, *with shorter bonds correlating with less positive (more negative) couplings* (Figure 8). The correlation, however, is imperfect in that the curves are slightly phase-shifted. This deviation apparently stems from the superimposed effects of r_{CH} *and* r_{CC} on $^2J_{CCH}$ (see below). In **2**, for example, the reduced $^2J_{C2,H1}$ at $\phi = -60°$ is caused by a smaller $r_{C1,C2}$ in this geometry (Figure 7), which shifts the *J*-coupling to more negative (less positive) values, as does a reduction in $r_{C1,H1}$. All of these effects are observed in the absence of an oxygen substituent at C2, which permits the isolation of energetic, structural, and *J*-coupling effects caused solely by ϕ rotation.

C. $^2J_{CCH}$ Spin-Couplings in 5−8. The effects of ϕ and α on computed $^2J_{C1,H2}$ and $^2J_{C2,H1}$ in **5**−**8** are shown in Figures 9−12. Computed $^2J_{C1,H2}$ displays a bimodal dependence on α, with minima at $\sim -30°$ and $\sim 150°$, and maxima at $\sim -120°$ and $\sim 60°$ for **5** and **6** (Figures 9A and 10A) and with minima at $\sim -150°$ and $\sim 30°$, and maxima at $\sim -60°$ and $\sim 120°$ for **7** and **8** (Figures 11A and 12A). Absolute couplings depend on ring configuration; for **5**, −2 to 6 Hz; for **6**, −7 to −3 Hz; for **7**, −3 to 4 Hz; for **8**, −2 to 3 Hz. A comparison of computed couplings to experimental values[18] in methyl glycosides **11**−**14** (Chart 3) shows generally good agreement. Changes in ϕ

(17) Tvaroska, I.; Bleha, T. In *Advances in Carbohydrate Chemistry and Biochemistry*; Tipson, R. S., Horton, D., Eds.; Academic Press: San Diego, CA, 1989; p 45.

(18) Podlasek, C. A.; Wu, J.; Stripe, W. A.; Bondo, P. B.; Serianni, A. S. *J. Am. Chem. Soc.* **1995**, *117*, 8635−8644.

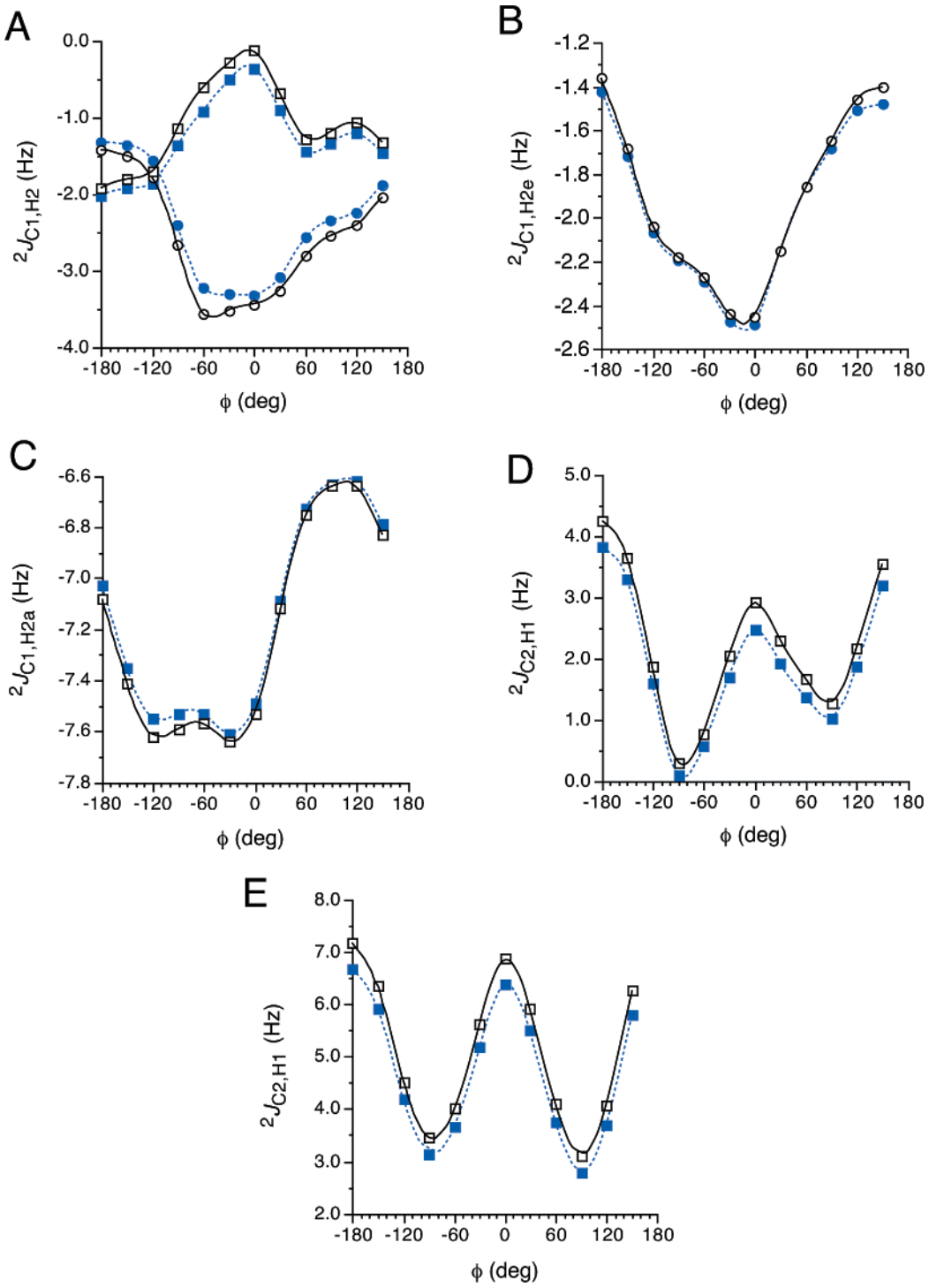

Figure 5. (A) Correlations between $^2J_{C1,H2}$ and ϕ in **1** (open symbols) and **3** (closed blue symbols). Squares, $^2J_{C1,H2a}$; circles, $^2J_{C1,H2e}$ (H2a = H2*S*; H2e = H2*R*; see Chart 2). (B) Correlations between $^2J_{C1,H2e}$ and ϕ in **2** (open circles) and **4** (closed blue circles). (C) Correlations between $^2J_{C1,H2a}$ and ϕ in **2** (open squares) and **4** (closed blue squares). (D) Correlations between $^2J_{C2,H1}$ and ϕ in **1** (open squares) and **3** (closed blue squares). (E) Correlations between $^2J_{C2,H1}$ and ϕ in **2** (open squares) and **4** (closed blue squares).

do not affect the shape of the curves correlating $^2J_{C1,H2}$ to α (the curves are essentially *y*-shifted).

$^2J_{C1,H2}$ in **5**−**8** is much less affected by ϕ than by α (Figures 9−12, panels A and B) (Chart 1; structure **III**). Consistent with this observation is that $^2J_{C2,H1}$ is considerably more affected by ϕ than by α (Figures 9−12, panels C and D). These results support the contention that C−O bond rotations involving the carbon *bearing the coupled proton* have a more pronounced effect on $^2J_{CCH}$ magnitude than do similar rotations *involving the coupled carbon*. Importantly, the effect of α on $^2J_{C2,H1}$ is relatively small (∼1 Hz) in **5**−**7** and only slightly larger in **8**. Plots of $^2J_{C2,H1}$ versus ϕ display two minima at ∼±90° and two maxima at ∼0° and ∼180°; in this respect, they mirror the behavior of standard Karplus curves relating ^3J to dihedral angle, although for $^2J_{CCH}$ the rotated bond is peripheral to the coupling pathway. Plots for **5**, **6**, and **8** are roughly symmetric about ϕ = 0°, whereas that for **7** shows significantly different *J*-couplings at the minima. The dynamic range is ∼5−6 Hz when

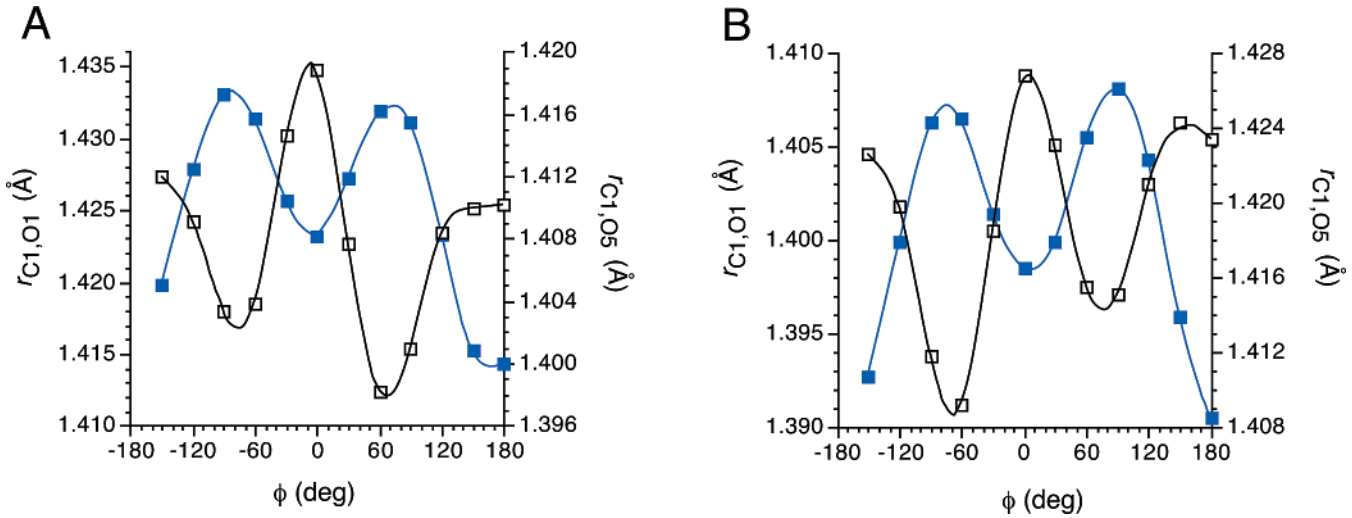

Figure 6. (A) Effect of ϕ on $r_{C1,O1}$ (open squares) and $r_{C1,O5}$ (closed blue squares) in **1**. (B) Effect of ϕ on $r_{C1,O1}$ (open squares) and $r_{C1,O5}$ (closed blue squares) in **2**.

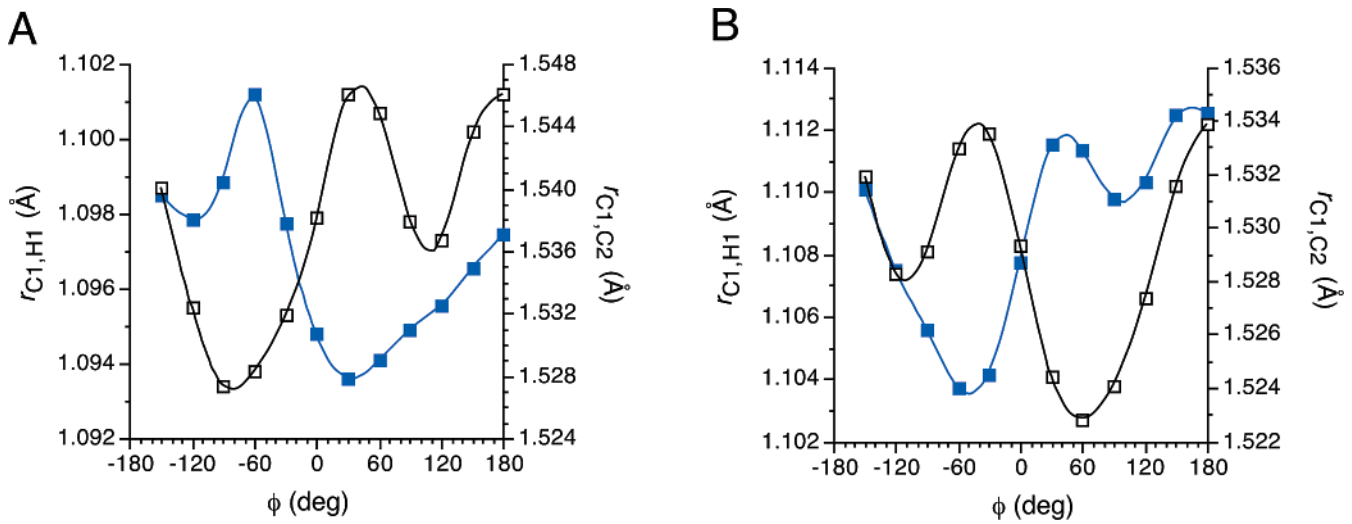

Figure 7. (A) Effect of ϕ on $r_{C1,H1}$ (open squares) and $r_{C1,C2}$ (closed blue squares) in **1**. (B) Effect of ϕ on $r_{C1,H1}$ (open squares) and $r_{C1,C2}$ (closed blue squares) in **2**.

Chart 3

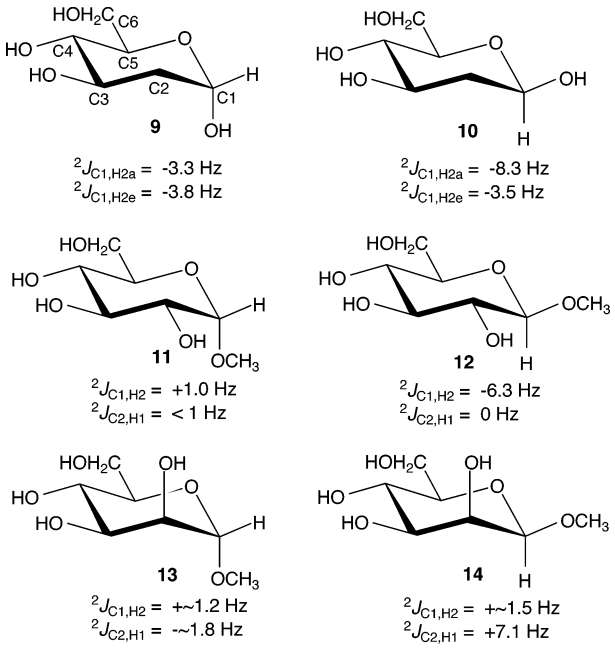

coupling signs are considered; for **5**, −2 to 3 Hz; for **6**, 0−5 Hz; for **7**, −4 to 2 Hz; for **8**, 7−13 Hz. *Absolute* $^2J_{C2,H1}$ values in **5**−**7** (2−5 Hz) are considerably smaller than that observed for **8** (7−13 Hz), in agreement with experimental couplings in **11**−**14** (Chart 3). Changes in α do not influence the shape of curves correlating $^2J_{C2,H1}$ with ϕ (the curves are essentially *y*-shifted); these results mirror those found for $^2J_{C1,H2}$ (see above).

The secondary torsional dependencies of $^2J_{C1,H2}$ (ϕ) and $^2J_{C2,H1}$ (α) are small (<~2 Hz) and essentially independent of the primary torsion (α and ϕ, respectively) (Figures 9−12, panels B and D).

D. Other Structural Factors Influencing $^2J_{CCH}$ in Saccharides. Plots of $r_{C1,H1}$ versus ϕ and $r_{C2,H2}$ versus α were evaluated in **5**−**8** (Figure S2) in an effort to identify structural factors responsible for the observed dependence of $^2J_{C2,H1}$ and $^2J_{C1,H2}$ on ϕ and α, respectively. Lone-pair effects on r_{CH} can be predicted from the results of prior work;[10b,19] vicinal oxygen lone pairs anti to the C−H bond lengthen these bonds due to

(19) (a) Kennedy, J.; Wu, J.; Drew, K.; Carmichael, I.; Serianni, A. S. *J. Am. Chem. Soc.* **1997**, *119*, 8933−8945. (b) Cloran, F.; Zhu, Y.; Osborn, J.; Carmichael, I.; Serianni, A. S. *J. Am. Chem. Soc.* **2000**, *122*, 6435−6448.

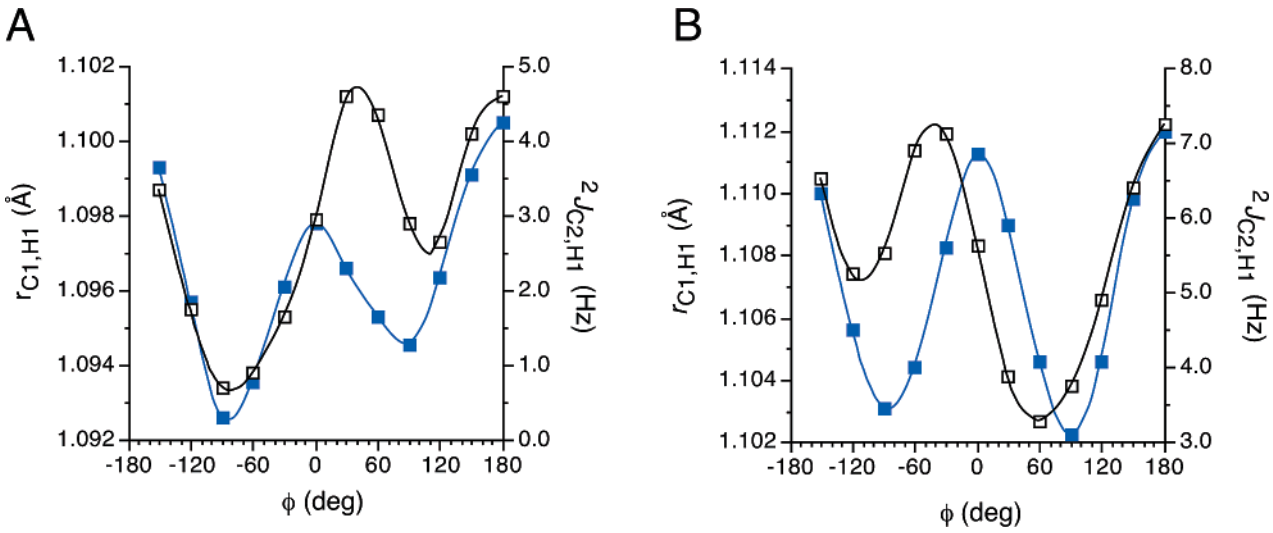

Figure 8. (A) Effect of ϕ on $r_{C1,H1}$ (open squares) and $^2J_{C2,H1}$ (closed squares) in **1**. (B) Effect of ϕ on $r_{C1,H1}$ (open squares) and $^2J_{C2,H1}$ (closed squares) in **2**.

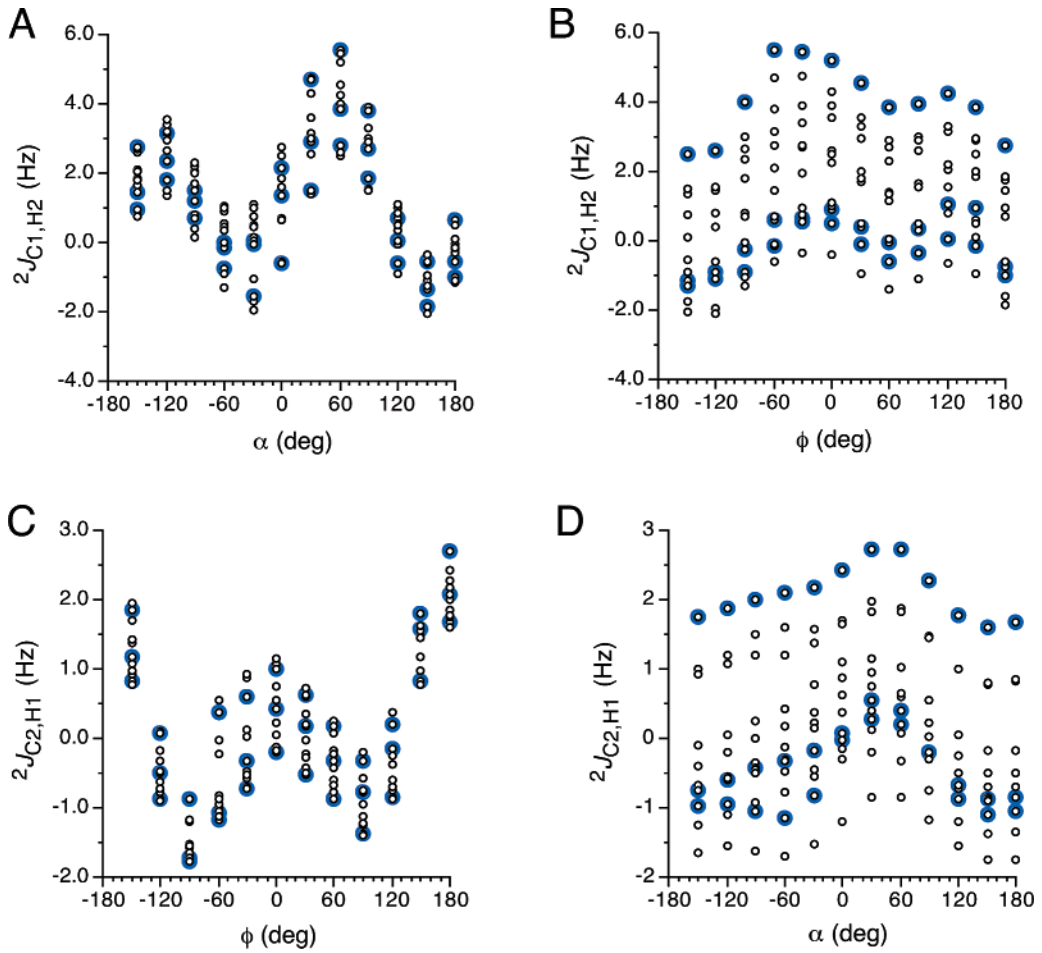

Figure 9. (A) Effect of α on $^2J_{C1,H2}$ in **5**. Point scatter at discrete values of α is due to the effect of ϕ; highlighted points (open blue circles) are for perfectly staggered values of ϕ. (B) Effect of ϕ on $^2J_{C1,H2}$ in **5**. Point scatter at discrete values of ϕ is due to the effect of α; highlighted points (open blue circles) are for perfectly staggered values of α. (C) Effect of ϕ on $^2J_{C2,H1}$ in **5**. Point scatter at discrete values of ϕ is due to the effect of α; highlighted points (open blue circles) are for perfectly staggered values of α. (D) Effect of α on $^2J_{C2,H1}$ in **5**. Point scatter at discrete values of α is due to the effect of ϕ; highlighted points (open blue circles) are for perfectly staggered values of ϕ.

lone-pair donation into the σ^* antibonding orbital on carbon (Scheme 1). On the basis of this model, $r_{C1,H1}$ is expected to be smaller in α-Glc **5** and α-Man **7** for ϕ near −60°, and in β-Glc **6** and β-Man **8** for ϕ near 60°. C−H bonds should be longer and of roughly equal length in the remaining two staggered ϕ rotamers. This trend is consistently observed (Figure S3A). Lone-pair effects on $r_{C2,H2}$ are as expected, with minima near $\alpha = -60°$ for α/β Glc and $\alpha = 60°$ for α/β Man (Figure S2B).

Superimposed on the above trends are the effects of ϕ rotation on $r_{C2,H2}$ (and presumably $r_{C2,O2}$) and of α rotation on $r_{C1,H1}$

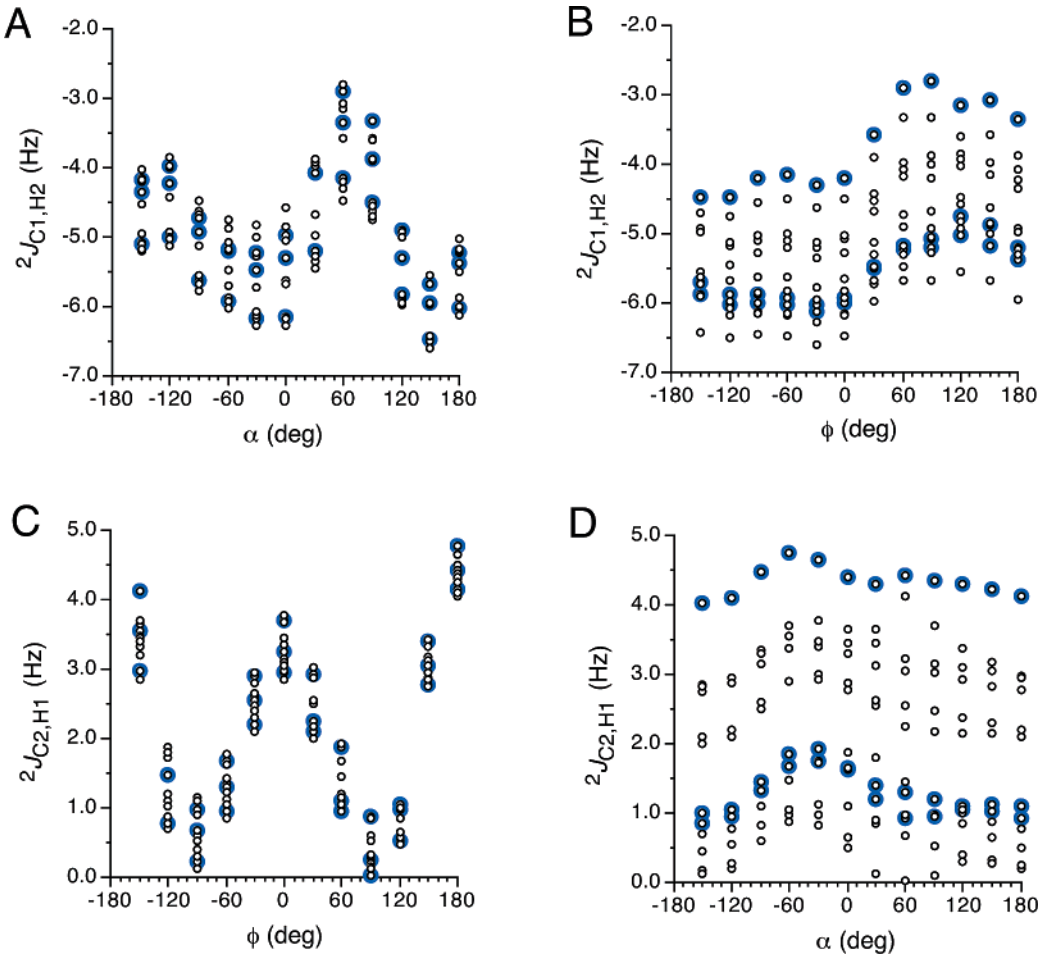

Figure 10. Same data as in Figure 9 for **6**.

(and presumably $r_{C1,O1}$), which were found to be consistent with prior relationships observed in furanosyl rings.[19] For perfectly staggered values of the rotated C−O torsion, 1,3-lone-pair effects were observed to reduce bond length. For example, $r_{C2,H2}$ is smaller for β-Glc **6** for $\phi = -60°$ and 180° than for $\phi = 60°$ (Scheme 1).

Equipped with the above-noted bond-length lone-pair relationships, the effects of the C1−C2−H2 and C2−C1−H1 bond angle on $^2J_{C1,H2}$ and $^2J_{C2,H1}$, respectively, were examined in **6** at perfectly staggered values of α and ϕ, respectively (Figure S3). A roughly linear dependence was observed for $^2J_{C1,H2}$; the coupling increases (i.e., becomes less negative) by ∼0.5 Hz per 1° increase in the bond angle regardless of the value of α (Figure S3A). This behavior is similar to that observed for $^2J_{HCH}$[20a] but differs from that reported for $^2J_{COC}$.[20b] For α = 60°, the curve is shifted by ∼2 Hz toward less negative couplings; in this rotamer, $r_{C2,H2}$ is larger due to the presence of an O2 lone pair anti to the C2−H2 bond. Interestingly, the curves for α = −60° and 180° *coincide* despite the presence of an oxygen lone pair anti to the C2−H2 bond in α = 180°. These results show that $^2J_{C1,H2}$ does not perfectly correlate with $r_{C2,H2}$. Similar observations were made for **5**, **7**, and **8** (data not shown).

$^2J_{C2,H1}$ in **6** appears less affected by ∠C2,C1,H1 (Figure S3B), although the dynamic range of the angle and the distribution of data points at each ϕ value are more limited. Couplings are similar for $\phi = 60°$ and −60° (1−2 Hz), but shift to more positive values (4−5 Hz) for $\phi = 180°$. For $\phi = -60°$ and 180°, an O1 lone pair is anti to the C1−H1 bond, yet significantly different $^2J_{C2,H1}$ values are observed. Thus, like $^2J_{C1,H2}$, $^2J_{C2,H1}$ magnitude does not perfectly correlate with $r_{C1,H1}$. Similar observations were made for **5**, **7**, and **8** (data not shown). These data also suggest that rotating ϕ significantly influences ∠C1,C2,H2, whereas ∠C2,C1,H1 is much less affected by rotating α.

Further inspection of $^2J_{CCH}$ versus r_{CH} data provides a possible explanation for the anomalous $^2J_{CCH}$ values in those C−O rotamers identified above (Figure S3). In these cases (e.g., α = 180° for $^2J_{C1,H2}$, and $\phi = -60°$ for $^2J_{C2,H1}$in **6**), the C−O torsion orients the hydroxyl proton anti to the coupled carbon; this geometry yields a smaller r_{C1-C2} since no oxygen lone pairs are anti to the bond. In these conformers, the reduced r_{C1-C2} shifts $^2J_{CCH}$ to a more negative value. Thus, *both the C−H and C−C bond lengths affect $^2J_{CCH}$, with shorter bonds leading to more negative (less positive) couplings.*

Studies of $^1J_{C1,H1}$ and $^1J_{C1,C2}$ in **5**−**8** as a function of r_{CH} and r_{CC} were also conducted by systematically varying bond lengths over a 0.02 Å range while optimizing the remaining parameters (only one combination of C1−O1 and C2−O2 bond torsions was inspected in each structure). $^1J_{CH}$ was found to vary roughly linearly with r_{CH},[10b] with shorter bonds yielding larger (more positive) couplings (Figure S4A). However, in some

(20) (a) Maciel, G. E.; McIver, J. W.; Ostlund, N. S.; Pople, J. A. *J. Am. Chem. Soc.* **1970**, *92*, 4151. (b) Cloran, F.; Carmichael, I.; Serianni, A. S. *J. Am. Chem. Soc*. **2000**, *122*, 396−397.

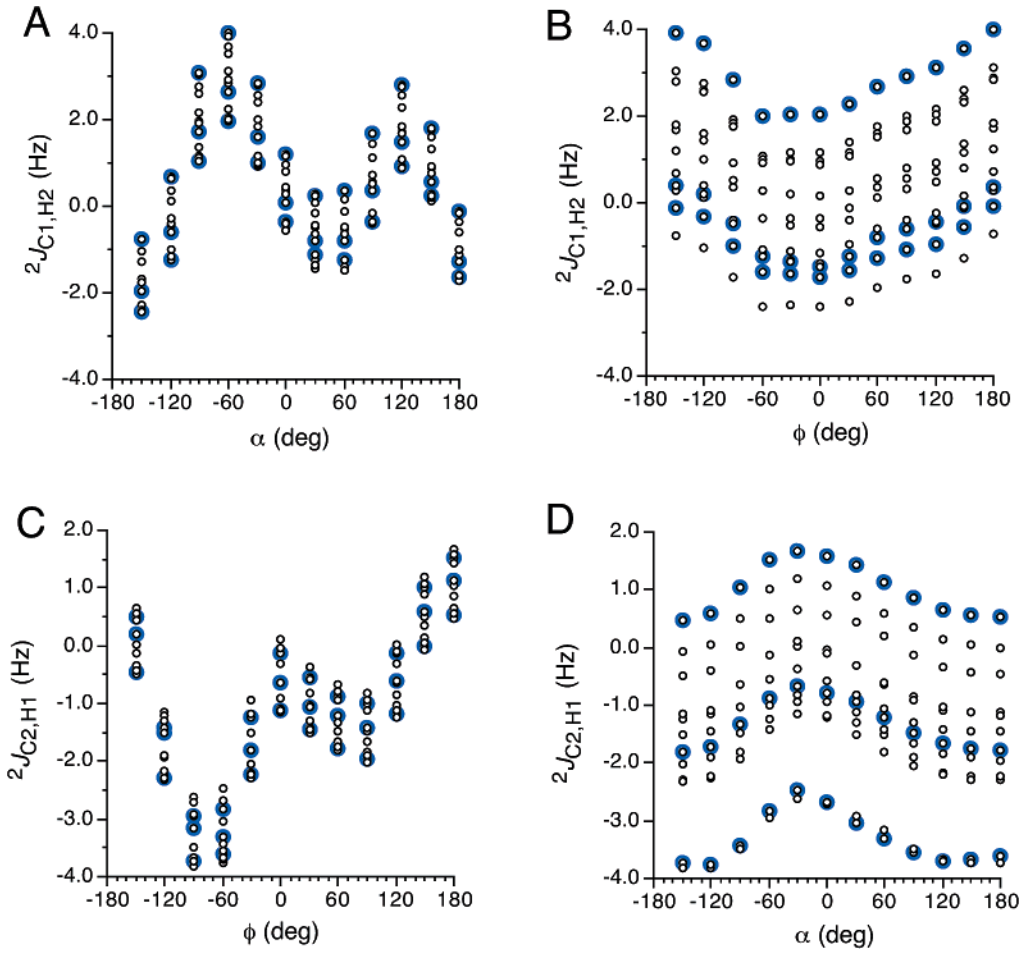

Figure 11. Same data as in Figure 9 for **7**.

cases, the dependence was very small (e.g., $^1J_{C1,H1}$ versus $r_{C1,H1}$ in α-Glc and α-Man). In contrast, the effect of $r_{C1,C2}$ on $^1J_{C1,H1}$ was strong in all cases; moderate changes in r_{CC} influence $^1J_{CH}$ values more significantly than do comparable changes in r_{CH} (Figure S4A). This observation may explain why correlations between r_{CH} and $^1J_{CH}$ were not uniformly observed in prior work;[10a] a critical r_{CC} factor is apparently operating and may dominate over effects caused by r_{CH}. $^1J_{CC}$ values decrease with increasing r_{CC} and are virtually unaffected by changes in r_{CH} on the coupled carbons (Figure S4B).

E. Quantitative Treatment of $^2J_{C1,H2}$ and $^2J_{C2,H1}$. Hypersurfaces relating $^2J_{C1,H2}$ and $^2J_{C2,H1}$ to ϕ and α in **5**−**8** are shown in Figures 13 and 14. These data were used to parameterize two equations relating $^2J_{C1,H2}$ and $^2J_{C2,H1}$ to ϕ and α.

$$^2J_{C1,H2} = A + B\cos\alpha + C\cos 2\alpha + D\sin\alpha + E\sin 2\alpha + F\cos\phi + G\cos 2\phi \quad (1)$$

$$^2J_{C2,H1} = A + B\cos\phi + C\cos 2\phi + D\sin\phi + E\sin 2\phi + F\cos\alpha + G\cos 2\alpha \quad (2)$$

Coefficients for eqs 1 and 2 are given in Table 1 for the four relative configurations at C1 and C2 of aldopyranosyl rings (**5**−**8**) and for the 2-deoxy-aldopyranosyl rings (**1**, **2**). The regular patterns in both torsional regimes permitted reasonable χ^2 and rms values to be obtained in the parameterizations. Single parameter equations were initially derived containing only the primary torsional variable (α for $^2J_{C1,H2}$; ϕ for $^2J_{C2,H1}$). A slightly better fit was obtained, however, with double-parameter equations containing two additional terms to treat the secondary torsional dependence (ϕ for $^2J_{C1,H2}$; α for $^2J_{C2,H1}$). The latter equations would be applicable if independent information on these secondary torsions is available (e.g., via $^3J_{HCOH}$ and/or $^3J_{CCOH}$ values).

Conclusions

$^2J_{CCH}$ values have received relatively little attention as conformational probes of saccharides in solution. However, recent studies of saccharide hydroxymethyl group conformation[9] suggest a wider role for these scalar couplings stemming from their sensitivities to both C−C and C−O torsion angles. For example, the C5−C6−H6*R*/*S* coupling pathways in aldohexopyranosyl rings yield $^2J_{CCH}$ values that are influenced by both the C5−C6 (ω) and C6−O6 (θ) torsion angles (**I**; Chart 1 and Figure 1). In this case, the remaining potential variable, the C5−O5 torsion angle, was fixed by the pyranosyl ring and thus played no role in modulating the couplings. In the present investigation, *the C−C torsion angle is held constant* by the pyranosyl ring, leaving both C−O torsions to potentially modulate the coupling. The present studies show that $^2J_{CCH}$ values are influenced by C−O torsion angles at both carbons of the C−C−H coupling pathway, but the effect is greater *at the carbon bearing the coupled proton*. The observation appears valid for both $^2J_{C1,H2}$ and $^2J_{C2,H1}$, suggesting that the nature of the coupled carbon (e.g., anomeric versus nonanomeric) is not important.

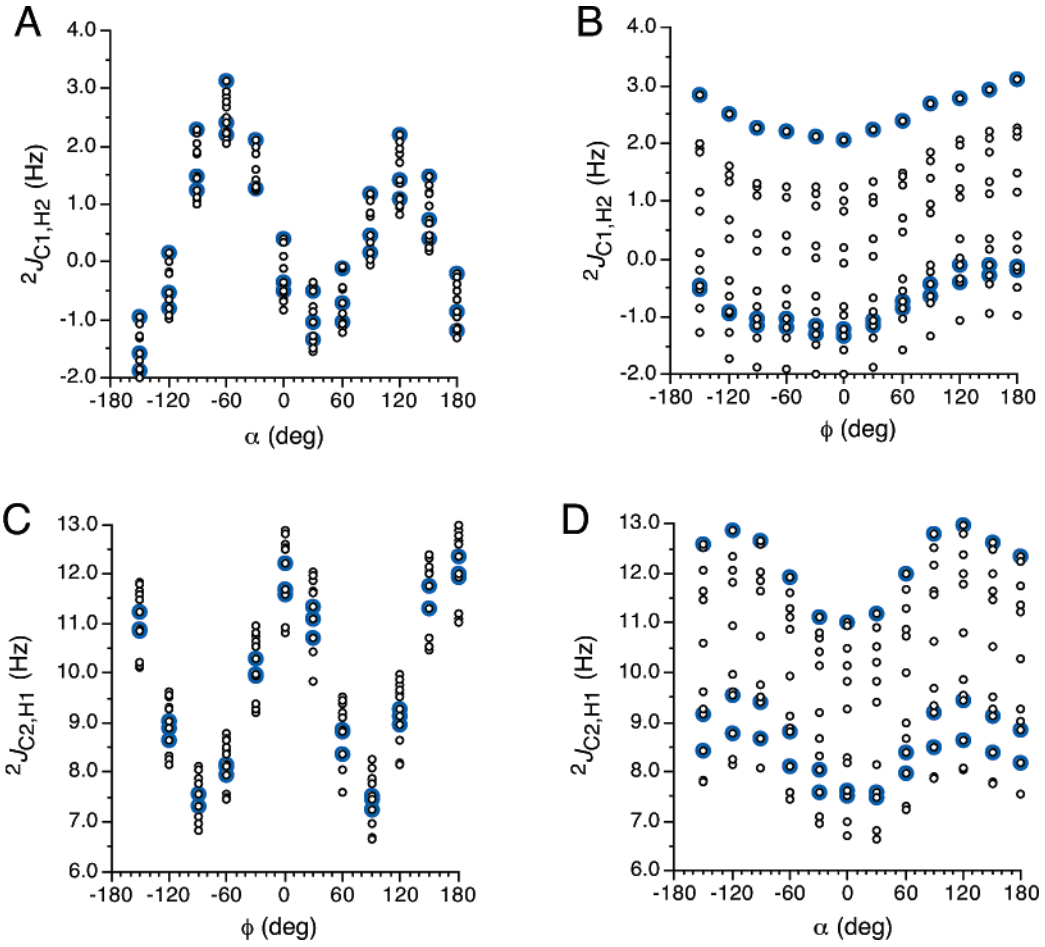

Figure 12. Same data as in Figure 9 for **8**.

Scheme 1

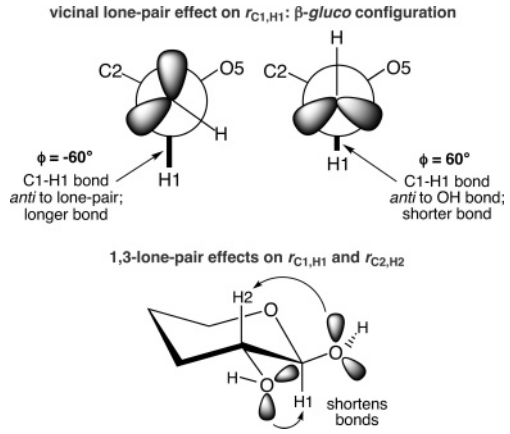

The effect of C−O bond rotation on $^2J_{CCH}$ appears to be mediated largely by oxygen lone-pair perturbations of C−H and C−C bond lengths. In general, reduction in the C−C and/or C−H bond lengths in the C−C−H coupling pathway shifts $^2J_{CCH}$ to more negative (less positive) couplings. Lone-pair effects appear mainly in two forms: vicinal effects (for the C1−H1, C2−H2, and C1−C2 bonds) and 1,3-effects (C1−H1 and C2−H2 bonds only), with the former resulting in bond length elongation and the latter causing bond length reduction. Because rotation of the C1−O1 and C2−O2 bonds induces lone-pair effects that may be reinforcing or canceling for any given bond, the dependence of $^2J_{CCH}$ on these torsions becomes a complex function of overlapping forces.

The expected vicinal lone-pair effects on $r_{C1,H1}$ and $r_{C2,H2}$ upon rotation of ϕ and α, respectively, are predicted consistently in **5**−**8**. This is not true for vicinal lone-pair effects on $r_{C1,C2}$; for example, rotating ϕ in **6** would be expected to increase $r_{C1,C2}$ for $\phi = 60°$ and 180° (O1 lone pair anti to the C1−C2 bond) relative to $\phi = -60°$, and that $r_{C1,C2}$ should be similar in the former group (Figure S2B). However, these trends are not consistently observed in **5**−**8** (data not shown), suggesting that oxygen lone-pair effects are modulated by other structural factors that may include competing stereoelectronic effects operating at the anomeric center and/or the presence of intramolecular H-bonding. The latter complication was cause for concern about $^2J_{CCH}$ computed in systems exhibiting H-bonding between O1 and O2, since C1−C2 bond length, a determinant of $^2J_{CCH}$, was observed to be sensitive to the presence of H-bonding (the presence of H-bonding between vicinal OH groups reduces r_{CC}). However, it is believed that this effect is small, based on the smooth, continuous character of computed $^2J_{CCH}$ versus ϕ/α curves for **5**−**8** and on the similarity of these curves to those found for **1** and **2**; in the latter structures, complications arising from intramolecular H-bonding are absent due to the lack of a vicinal diol fragment at C1 and C2. It is also noted that 1,3-lone-pair effects on $r_{C1,H1}$ and $r_{C2,H2}$ are consistently observed in **5**−**8** as suggested from prior studies in furanosyl rings,[19] although there are exceptions attributed again to the presence of H-bonding in the structure.

New equations correlating $^2J_{C1,H2}$ and $^2J_{C2,H1}$ with ϕ and/or α in aldopyranosyl rings have been derived. $^2J_{C2,H1}$ has particular

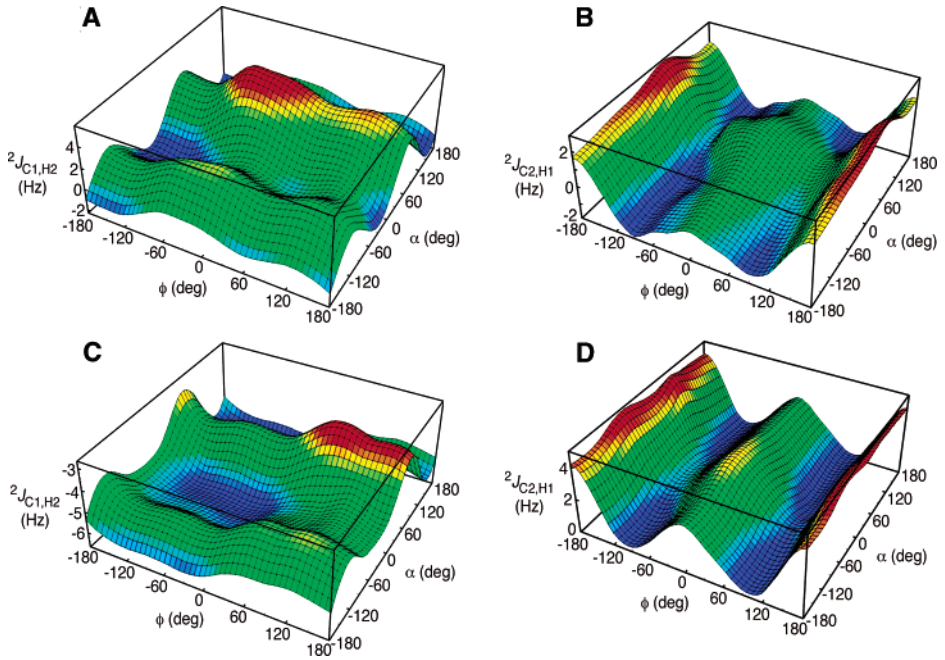

Figure 13. Computed hypersurfaces showing the dependencies of $^2J_{C1,H2}$ and $^2J_{C2,H1}$ on ϕ and α in **5** (A and B, respectively), and in **6** (C and D, respectively).

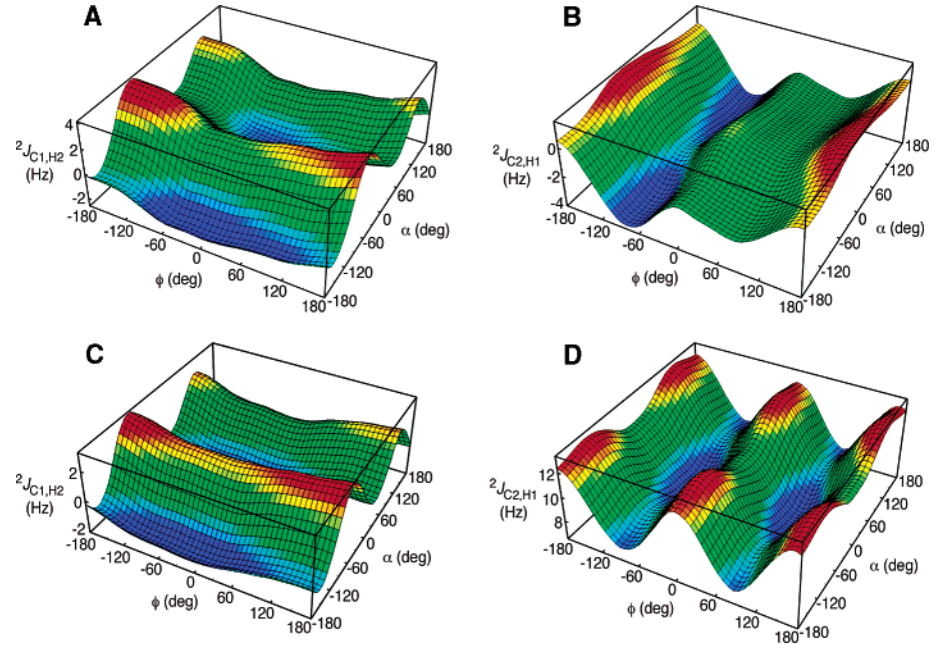

Figure 14. Computed hypersurfaces showing the dependencies of $^2J_{C1,H2}$ and $^2J_{C2,H1}$ on ϕ and α in **7** (A and B, respectively), and in **8** (C and D, respectively).

relevance for studies of oligosaccharide conformation wherein assessments of preferred conformation about ϕ are important. These couplings can be measured in specific monosaccharide residues labeled with ^{13}C at C2, since signal multiplicity at the well-resolved adjacent anomeric proton can be observed readily. Alternatively, natural abundance methods for J_{CH} measurements could be applied.[21] Recent work has suggested that *trans*-glycoside *J*-couplings yield quantitative information about C−O rotamer populations in glycosidic linkages.[22] However, evaluations of ϕ appeared less firm than those of ψ due to use of the less reliable (and less sensitive) *trans*-glycoside $^2J_{COC}$. $^2J_{C2,H1}$ may provide an additional means of evaluating ϕ. Since $^2J_{C2,H1}$ displays some sensitivity to α, however, more accurate treatments of $^2J_{C2,H1}$ in oligosaccharides may require an independent evaluation of the C2−O2 torsion angle. The latter could be obtained from measurements of $^3J_{HCOH}$[23] or $^3J_{CCOH}$[24] in solution. In residues lacking a hydroxyl group at C2 (i.e., 2-deoxyaldopyranosyl rings), application of $^2J_{C2,H1}$ to evaluate ϕ should be more straightforward.

(21) (a) Meissner, A.; Sørensen, O. W. *Magn. Reson. Chem.* **2001**, *39*, 49−52. (b) Blechta, V.; del Rio-Portilla, F.; Freeman, R. *Magn. Reson. Chem.* **1994**, *32*, 134−137. (c) Nishida, T.; Widmalm, G.; Sandor, P. *Magn. Reson. Chem.* **1995**, *33*, 596−599.

(22) (a) Cloran, F.; Carmichael, I.; Serianni, A. S. *J. Am. Chem. Soc.* **1999**, *121*, 9843−9851. (b) Thibaudeau, C.; Klepach, T.; Zhao, S.; Reed, M.; Carmichael, I.; Serianni, A. S. To be submitted for publication.

(23) Fraser, R. R.; Kaufman, M.; Morand, P.; Govil, G. *Can. J. Chem.* **1969**, *47*, 403−409.

(24) Dais, P.; Perlin, A. S. *Can. J. Chem.* **1982**, *60*, 1648.

Table 1. Coefficients in Parameterized Equations for $^2J_{C1,H2}$ and $^2J_{C2,H1}$ in **1**, **2**, and **5**−**8**, and χ^2 and RMS Values Derived from the Fit

	α-Glc **5** $^2J_{C1,H2}$	α-Glc **5** $^2J_{C2,H1}$	β-Glc **6** $^2J_{C1,H2}$	β-Glc **6** $^2J_{C2,H1}$	α-Man **7** $^2J_{C1,H2}$	α-Man **7** $^2J_{C2,H1}$	β-Man **8** $^2J_{C1,H2}$	β-Man **8** $^2J_{C2,H1}$	α-deoxyGlc **1** $^2J_{C2,H1}$	β-deoxyGlc **2** $^2J_{C2,H1}$
					Single Parameter					
A	1.30	0.086	−5.07	2.05	0.50	−1.17	0.30	9.88	2.24	5.12
B	0.13	0.50	0.16	0.062	−0.67	1.21	−0.50	0.37	0.69	0.044
C	−1.15	−0.60	−0.41	−0.92	1.74	−0.77	1.64	−1.23	−0.79	−1.05
D	−0.81	0.50	−0.25	0.38	−0.31	0.39	−0.11	0.16	0.49	0.26
E	−1.63	0.99	−0.79	1.40	0.053	1.01	0.042	1.89	1.11	1.55
χ^2	106.1	32.6	42.0	19.9	68.3	29.0	25.8	61.6	0.19	0.09
rms (Hz)	0.74	0.23	0.29	0.14	0.48	0.20	0.18	0.43	0.02	0.01
					Double Parameter					
A	1.30	0.086	−5.07	2.05	0.50	−1.17	0.30	9.88		
B	0.13	0.50	0.16	0.062	−0.67	1.21	−0.50	0.37		
C	−1.15	−0.60	−0.41	−0.92	1.73	−0.77	1.64	−1.23		
D	−0.81	0.50	−0.25	0.38	−0.31	0.39	−0.11	0.16		
E	−1.63	0.99	−0.79	1.40	0.053	1.01	0.042	1.89		
F	−0.17	−0.11	0.65	−0.21	0.40	−0.37	0.45	0.29		
G	0.56	−0.17	0.10	0.13	−0.24	0.067	0.039	0.27		
χ^2	81.7	29.7	11.0	15.4	52.6	18.9	11.0	50.6		
rms (Hz)	0.57	0.21	0.08	0.11	0.37	0.13	0.08	0.35		

While this report has focused on $^2J_{CCH}$ values as constraints for ϕ in glycosides, similar couplings may also be applicable to ψ analysis. For example, in β-(1 → 4) linkages, $^2J_{C3,H4}$ and $^2J_{C5,H4}$ may serve as additional ψ constraints, assuming that they obey the same dependencies on C−O torsions as observed for $^2J_{C2,H1}$. This application remains to be explored.

The predicted behavior of $^2J_{C1,H2}$ and $^2J_{C2,H1}$ reported herein was deduced from studies of *J*-couplings in gas-phase molecules. It is thus possible that *J*-coupling behavior in aqueous solution may be influenced by the presence of H-bonding between saccharide hydroxyl groups and solvent water. $^1J_{CH}$ values are reported to display a solvent dependence,[25] while $^3J_{CH}$ values are expected to be considerably less affected by solvent. $^2J_{CCH}$ may display an intermediate solvent dependency, although this has not been tested computationally or experimentally. However, even if solvation affects $^2J_{CCH}$, the overall *trends* reported here are expected to be maintained, with possible changes manifested in curve amplitude shifts (i.e., the absolute values of $^2J_{CCH}$ will be uniformly shifted but overall dependencies will be maintained).

Given the dual dependence of $^2J_{CCH}$ on C−O torsions on both carbons along the coupling pathway, a concerted analysis of multiple $^2J_{CCH}$ values within specific aldopyranosyl rings may lead to a more complete picture of C−O torsional preferences in solution. Thus, for example, if the eight intra-ring $^2J_{CCH}$ within **6** ($^2J_{C1,H2}$, $^2J_{C2,H1}$, $^2J_{C2,H3}$, $^2J_{C3,H2}$, $^2J_{C3,H4}$, $^2J_{C4,H3}$, $^2J_{C4,H5}$, $^2J_{C5,H4}$) were properly parameterized and if all values were known experimentally, then the eight equations could be collectively solved to extract "best fit" C−O torsions in solution. These data could be compared or combined with other information (e.g., from $^3J_{HCOH}$ and/or $^3J_{CCOH}$) to improve the reliability of the conclusions. Thus, $^2J_{CCH}$ not only reports *on relative configuration* along the C−C−H pathway, as demonstrated by the empirical rules developed by Perlin[7,8] and Pedersen,[6] but also holds the potential of indirectly evaluating C−O torsions in saccharides for both C−O−R and C−O−H fragments.

Acknowledgment. This work was supported by grants from Omicron Biochemicals, Inc. of South Bend, IN, and the National Institutes of Health (GM) (to A.S.). The Notre Dame Radiation Laboratory is supported by the Office of Basic Energy Sciences of the United States Department of Energy. This is Document No. NDRL-4530 from the Notre Dame Radiation Laboratory.

Supporting Information Available: Four figures showing ϕ/α population contour maps for **5**−**8** derived from DFT-calculated total energies (Figure S1), correlations between $r_{C1,H1}$, $^2J_{C2,H1}$, and ϕ, and between $r_{C2,H2}$, $^2J_{C1,H2}$, and α in **6** (Figure S2), correlations between C−C−H bond angle and $^2J_{C1,H2}$ and $^2J_{C2,H1}$ in **6** (Figure S3), and correlations between $r_{C1,H1}$ and $^1J_{C1,H1}$, and between $r_{C1,C2}$ and $^1J_{C1,C2}$, in **6** either in fully optimized structures or in structures containing incremented (and fixed) C1−H1 or C1−C2 bond lengths (Figure S4). This material is available free of charge via the Internet at http://pubs.acs.org.

JA040251Y

(25) Zaccari, D. G.; Snyder, J. P.; Peralta, J. E.; Taurian, O. E.; Contreras, R. H.; Barone, V. *Mol. Phys.* **2002**, *100*, 705−715.